Insights into evapotranspiration partitioning based on hydrological observations using the generalized proportionality hypothesis

Amin Hassan[1], I. Colin Prentice[2,3], Xu Liang[1]

[1]Department of Civil and Environmental Engineering, University of Pittsburgh, Pittsburgh, Pennsylvania, 15213, USA

5 [2]Georgina Mace Centre for the Living Planet, Department of Life Sciences, Imperial College London, Silwood Park Campus, Ascot, UK

[3]Department of Earth System Science, Ministry of Education Key Laboratory for Earth System Modeling, Institute for Global Change Studies, Tsinghua University, Beijing, China

10 *Correspondence to*: Xu Liang (xuliang@pitt.edu)

Abstract. Evapotranspiration (ET) comprises transpiration, soil evaporation, and interception. The partitioning of ET is challenging due to the lack of direct measurements and uncertainty of existing ET partitioning methods. We propose a novel method to estimate long-term mean transpiration to evapotranspiration (T/ET) ratios based on the generalized proportionality hypothesis using long-term mean hydrological observations at the watershed scale. We tested the method using 648 watersheds

15 in the United States classified into six vegetation types. We mitigated impacts of the variability associated with different PET data products by rescaling their original PET values using the product ET/PET ratios in combination with the observed ET calculated from watershed water balance. With PET thus rescaled, our method produced consistent T/ET across six widely used PET products. Shrubs (0.38) and grasslands (0.33) showed lower mean T/ET than croplands (0.46) and forests (respectively 0.73, 0.55, and 0.68 for evergreen needleleaf, deciduous broadleaf, and mixed forests). T/ET showed significant

20 dependence on aridity, leaf area index, and other hydrological and environmental conditions. Using T/ET estimates, we calculated transpiration to precipitation ratios (T/P) ratios and revealed a bell-shaped curve at the watershed scale, which conformed to the bell-shaped relationship with the aridity index (AI) observed at the field scale (Good et al., 2017). This relationship peaked at a T/P between 0.5 and 0.6, corresponding to an AI between 2 and 3 depending on the PET dataset used. These results strengthen our understanding of the interactions between plants and water and provide a new perspective on a

25 long-standing challenge for hydrology and ecosystem science.

1 Introduction

Partitioning evapotranspiration (ET) is important for understanding water and energy balances of terrestrial ecosystems. ET has been predicted to increase at the expense of soil moisture due to climate change (Li et al., 2022; Niu et al., 2019) with potential implications for future projections of water, energy, and carbon balances. Large uncertainty remains in the

30 partitioning of ET into its components: transpiration, interception, and bare soil evaporation. Various methods have been developed to partition ET based on measurements (Kool et al., 2014; Stoy et al., 2019). These include (1) flux-variance

similarity methods using high frequency (10–20 Hz) flux tower measurements, which estimate T/ET based on carbon-water correlation since transpiration and plant carbon uptake are concurrent (Scanlon and Kustas, 2012, 2010; Scanlon and Sahu, 2008; Skaggs et al., 2018); (2) eddy-covariance methods, which estimate T/ET using assumptions related to water use

35   efficiency based on widely available half-hourly/hourly eddy covariance measurements (Berkelhammer et al., 2016; Li et al., 2019; Scott and Biederman, 2017; Yu et al., 2022; Zhou et al., 2016) ; and (3) isotopic methods (Griffis, 2013; Williams et al., 2004; Zhang et al., 2011). Measurements of sap flow through plant stems have also been commonly used to more directly estimate transpiration. Sap flow measurements are classified into three groups (Kool et al., 2014): heat balance methods (Čermák et al., 1973; Sakuratani, 1987, 1981), heat pulse methods (Cohen et al., 1981; Green et al., 2003; Swanson and

40   Whitfield, 1981), and constant heater methods (Čermák et al., 2004; Granier, 1985). Poyatos et al. (2021) compiled 202 sap flow datasets to form the global SAPFLUXNET dataset. Recent studies have used remotely sensed solar-induced fluorescence (SIF) measurements (Alemohammad et al., 2017; Damm et al., 2018; Liu et al., 2022; Lu et al., 2018; Pagán et al., 2019; Shan et al., 2019) as a way to estimate global transpiration, relying on the close coupling between transpiration and photosynthesis. The ratio of transpiration to evapotranspiration (T/ET) is a particularly important quantity because the controls on T (which is

45   tightly regulated by plants through stomatal behaviour) are substantially different from the controls on the other two components. The ET partitioning methods summarized above have multiple limitations and produce an alarmingly wide range of values for the global mean T/ET. Wei et al. (2017) showed mean global T/ET varying from 0.24 to 0.90 based on a variety of remote-sensing, isotopic, and modelling studies. Another compilation by Liu et al. (2022) showed the mean varying between 0.24 and 0.86. Schlesinger and Jasechko (2014) showed that T/ET ratios derived from isotopic methods tend to be

50   systematically higher than those produced by other methods. It has also been shown that two different ET partitioning methods could produce greatly different T/ET values at the same site (Cavanaugh et al., 2011; Moran et al., 2009). Some T/ET estimates at the stand scale ignore transpiration from subcanopy vegetation, resulting in underestimation (Schlesinger and Jasechko, 2014). There is no consensus on which method is more accurate (Stoy et al., 2019); this presents a challenge for applying the T/ET estimates using any of the above methods, especially when they are developed based on data at site scale but are applied

55   at larger (regional to global) spatial scales.

Few studies have considered partitioning ET based on hydrological concepts using widely available long-term hydrological observations, which could in principle provide reliable methods to estimate T/ET. Gerrits et al. (2009) estimated monthly and (upscaled) annual transpiration based on precipitation, interception, soil moisture, and the aridity index. Mianabadi et al. (2019) extended their approach and applied it globally. In this study, we propose a new method to partition ET based on the

60   Generalized Proportionality Hypothesis (GPH) using long-term hydrological observations. The GPH was initially used by the United States Soil Conservation Service (SCS) for runoff calculation (USDA SCS, 1985), and was afterwards generalized by Ponce and Shetty (1995a, 1995b). Wang and Tang (2014) provided a comprehensive discussion of the use of GPH and noted its connection to various models, including the "abcd" model, the SCS direct runoff model, and the Budyko-type models. The GPH partitions water fluxes into their components and has been implemented as a two-stage partitioning. The first stage

65   partitions precipitation into soil wetting and surface runoff; the second stage partitions soil wetting into baseflow and

evaporation (Ponce and Shetty, 1995a, 1995b; Tang and Wang, 2017). We follow an approach based on the GPH partitioning of soil wetting to estimate catchment T/ET based on hydrological observations. Due to the wider availability of hydrological observations compared to the observations required for the techniques previously mentioned, this method has a wide potential for application in gauged watersheds across the globe.

70 The objectives of our study are: 1) to develop a new method to estimate T/ET at the catchment scale based on long-term hydrological observations, 2) to test the method and evaluate its robustness to different data products using watersheds with different vegetation types, 3) to find T/P (transpiration/precipitation) ratios based on T/ET and to compare this to previous studies, and 4) to understand the effect of hydrological and environmental conditions on both T/ET and T/P. The paper is organized as follows. Section 2 describes the newly developed method. Section 3 describes datasets used. Section 4 presents

75 results from the new method and compares them with T/ET estimates from other studies. Section 5 discusses the results and investigates their dependence on hydrological and environmental factors. Section 6 provides an insight into the variation of some existing partitioning methods. Section 7 summarizes our conclusions.

2 Methods and Data

2.1 Theory

80 We present a new method to estimate long-term mean T/ET ratios at a watershed scale by taking advantage of long-term available hydrological observations. The new method is based on the Generalized Proportionality Hypothesis (GPH), shown in equation (1). GPH partitions an unbounded water quantity Z into an unbounded water quantity Y and a water quantity X that is bounded by its potential value X_p. The value X_0 is the initial quantity of X that is fulfilled prior to the competition between X and Y; for example, interception is a portion of ET that is initially lost and not accessible for baseflow:

$$\frac{X - X_0}{X_p - X_0} = \frac{Y}{Z - X_0} \tag{1}$$

85 Ponce and Shetty (1995a, 1995b) applied the GPH for hydrological partitioning. They partitioned long-term mean precipitation into soil wetting and direct runoff, and further partitioned soil wetting into baseflow and runoff. The partitioning of soil wetting (W) into baseflow (Q_b) and evapotranspiration (ET) is shown in equation (2):

$$\frac{ET - ET_0}{PET - ET_0} = \frac{Q_b}{W - ET_0} \tag{2}$$

where ET_0 is the initial evapotranspiration that does not compete with baseflow and PET is the potential evapotranspiration. W can be estimated as $P - Q_d$, where P is precipitation and Q_d is direct runoff. ET can be estimated as $P - Q$, where Q is the

90 total runoff (since the long-term mean soil moisture change can be ignored). Initial evapotranspiration (ET_0) is assumed to be a fraction λ of the total evapotranspiration (ET), leading to equation (3):

$$\frac{ET - \lambda ET}{PET - \lambda ET} = \frac{Q_b}{W - \lambda ET} \tag{3}$$

We assume ET_0 differs in humid and arid regions. For humid regions, ET_0 includes bare soil evaporation and interception only, and therefore the ratio of transpiration to total evapotranspiration (T/ET) for humid regions becomes $1 - \lambda$. On the other hand, for arid regions, we assume that ET_0 includes bare soil evaporation, interception, and a portion (f) of the transpiration (T) representing the transpiration from the top 10 cm of soil (Abeshu and Li, 2021; Savenije, 2004). Since the atmospheric demand is high in arid regions, and since root uptake occurs near the surface and progresses downwards (Gardner, 1983), we assume that transpiration extracted from the topsoil occurs in a rapid manner that makes it inaccessible to the competition between baseflow and ET, and therefore is a part of ET$_0$. The remaining portion of ET after deducting ET_0 is equivalent to the remaining portion of T after deducting the portion f:

$$(1 - \lambda)ET = (1 - f)T \tag{4}$$

Therefore, the transpiration ratio (T/ET) for arid regions becomes:

$$\frac{T}{ET} = \frac{1 - \lambda}{1 - f} \tag{5}$$

Equation (5) indicates that T/ET can be found using λ and f values. λ can be found by applying an optimization technique that maximizes the non-parametric Kling-Gupta efficiency (KGE, equation 6) (Gupta et al., 2009; Pool et al., 2018) between observed soil wetting and simulated soil wetting:

$$KGE = 1 - \sqrt{(r - 1)^2 + (\alpha - 1)^2 + (\beta - 1)^2} \tag{6}$$

r: Pearson correlation coefficient

α: relative variability in the simulated and observed values

β: ratio between the mean simulated and mean observed flows

$$W_{obs} = P - Q_d \tag{7}$$

$$W_{sim} = Q_b \frac{PET - \lambda ET}{ET - \lambda ET} + \lambda ET \tag{8}$$

2.2 Data

From Equations 2-5 and the descriptions of Section 2.1, we see that one needs long-term observed precipitation, streamflow, baseflow, estimated PET, and root distribution to estimate the T/ET ratio. Watershed boundaries and precipitation data were retrieved from the Hydrometeorological Sandbox - École de technologie supérieure (HYSETS) dataset (Arsenault et al., 2020). The HYSETS dataset includes watershed boundaries, land cover, soil properties, meteorology, and hydrological data for 14,425 watersheds in North American. We selected 648 watersheds (Fig. 1) across the United States with at least 10 years of streamflow data between 1980 and 2018 from this HYSETS data source. Detailed land cover data were retrieved from the ESA CCI Land Cover project (www.esa-landcover-cci.org, last accessed December 28, 2022).

Streamflow data were retrieved from the US Geological Survey (USGS), while their corresponding baseflow magnitudes were estimated by separating it from the streamflow data in which a one-parameter digital filter separation method -- the Web-based

Hydrological Analysis Tool (WHAT) – was applied (Lim et al., 2010, 2005, https://engineering.purdue.edu/mapserve/WHAT,

115 last accessed 25 Oct 2022). The value of the filter parameter was taken as 0.925. Details on the baseflow separation method are presented in Lim et al. (2005). Information related to root density functions was obtained from Zeng (2001), who represented root density distribution as a two-parameter function for each vegetation type based on compiled root database. The root density distribution from Zeng (2001) was validated using root information from other studies (Fan et al., 2016; Jackson et al., 1996; Lozanova et al., 2019; Schenk and Jackson, 2002; Wallace et al., 1980). Soil moisture stress (Q_b/Q) was

120 calculated based on the USGS observed streamflow and the estimated baseflow from WHAT.

Numerous PET data products are available that satisfy our study regions and time period requirements, posing a question as to which should be selected – as each has its own strengths. To address this question, we examined six widely used PET data products and assessed their impact on the estimation of T/ET ratios. These data products were selected because they are (1) widely used within the hydrological and ecological communities, (2) associated with a wide range of spatial resolutions, and

125 (3) derived using different methods. The six PET datasets are the Global Land Evaporation Amsterdam Model (GLEAM v3.5a) (Martens et al., 2017), the Moderate Resolution Imaging Spectroradiometer (MODIS MOD16A3GF) product (Running et al., 2021), the dataset from Zhang et al. (2010), the North American Regional Reanalysis (NARR) (Mesinger et al., 2006), the Simple Process-Led Algorithms for Simulating Habitats (SPLASH v1.0) (Davis et al., 2017), and the Breathing Earth System Simulator (BESS v2) (Li et al., 2023). Details of these six products are provided in Table 1.
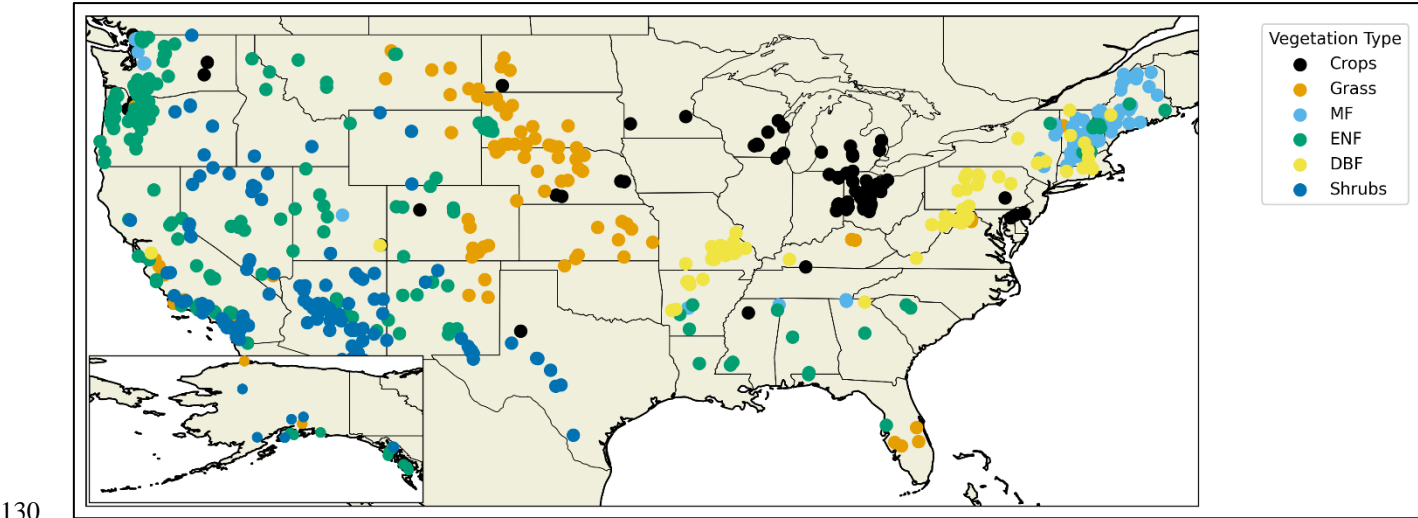

130

Figure 1: 648 watersheds in the US, categorized into six vegetation types; crops, grass, shrubs, evergreen needleleaf forest (ENF), deciduous broadleaf forests (DBF), and mixed forests (MF). The inset map at the bottom left shows watersheds in Alaska.

Table 1: Description of six PET products used in this study.

Dataset	PET equation	Spatial and temporal scale	Remarks

GLEAM v3.5a	Priestley-Taylor	0.25×0.25°, Daily/Monthly, 1980-2021	
NARR	Eta Model (Penman based)	32×32 km, Daily/Monthly, 1979-2022	
MODIS MOD16A3GF	Combination of Penman-Monteith and Priestley-Taylor	500×500m, 8-day/Yearly, 2000-2021	
SPLASH	Priestly-Taylor	1 km, Daily, 1980-2018	Forced using daily DayMet (Thornton et al., 2022) data
BESS v2	Priestly-Taylor	5 km, Monthly, 1982-2022	
Zhang	Penman-Monteith	8×8 km, Daily/Monthly, 1983-2006	

135 Environmental variables – relative humidity, downward shortwave radiation, air temperature, wind speed, and soil moisture content – were retrieved from the NARR dataset to study the dependencies of T/ET on environmental factors. Data on leaf area index (LAI) were obtained from ORNL DAAC (Mao and Yan, 2019) and aggregated to obtain the long-term mean LAI at watershed scale.

The relevant data were collected for 648 watersheds and aggregated to the annual timescale. The dominant vegetation type

140 was determined for each watershed from the ESA CCI land cover data, and watersheds were classified into six vegetation types: crops, grass, shrubs, evergreen needleleaf forest (ENF), deciduous broadleaf forest (DBF), and mixed forest (MF). We assume each watershed has a single mean long-term T/ET value. For each dataset, due to the different time coverage of the datasets and the streamflow gauges, we filtered the watersheds to include only those that have available data for at least 10 years. We used optimization to find λ. We then performed additional filtering for each dataset to remove watersheds with KGE

145 values less than zero. Using the filtered watersheds, we calculated T/ET based on estimated λ and f together with the other variables. The final number of watersheds associated with each dataset used in this study, after filtering, is shown in Table 2.

Table 2: Number of filtered watersheds for each potential evapotranspiration (PET) data product. Watersheds with less than 10 years of data and/or with Kling-Gupta efficiencies less than zero were removed from the analysis. Numbers are shown for each of the six vegetation types.

Type	All watersheds	NARR	MODIS	Zhang	GLEAM v3.5a	BESS v2	SPLASH
Crops	74	72	61	57	73	59	71

Grass	89	84	66	73	86	79	81
Shrubs	146	131	107	114	134	128	131
ENF	206	166	118	118	173	161	156
DBF	65	65	61	54	65	64	65
MF	68	63	58	52	66	51	61
Total	**648**	**581**	**471**	**468**	**597**	**542**	**565**

3 Impact of PET products

Figure 2a shows mean annual PET values from six different data products for the 648 study watersheds. We observe large differences in mean annual PET among the six different data products. The differences in PET are likely attributed to variations in input data and parameter values used by these products, while differences in methods and resolutions used to compute PET may play a secondary role (Hassan et al., 2024). Discrepancies between the input net radiation used in different data products result in especially large variations in the computed PET. Variations in parameter values, including the Priestly-Taylor α parameter, among different data products also result in significant differences in the resulting PET. On the other hand, the ET/PET ratios from the six different PET products are relatively consistent among the six datasets (except for GLEAM) as shown in Figure 2b. This is likely because within each product the same input/forcing data and parameter values are employed for both PET and ET, resulting in similar impacts on both. Such consistency is an indication of a uniformity of the underlying physics across these five products, despite the large disparities in their PET magnitudes. The GLEAM PET product, which has also been previously identified for its overestimation of ET/PET ratio by Peng et al. (2019) in comparison with FLUXNET ET/PET, appears to be an exception. Rather than excluding the GLEAM data product, we opted to rescale its ET/PET ratio (referred to as rescaling factor) by normalizing it with the average ratio of the other five datasets (NARR, MODIS, Zhang, SPLASH, and BESS), yielding a rescaling factor of 0.7. This rescaling factor of 0.7 was applied to GLEAM to derive new PET data, using watershed ET values (referred to as observed ET hereafter) obtained from the water balance equation with observed long-term mean precipitation and streamflow data. Similarly, PET values for the other five data products in this study were newly derived by applying their individual ET/PET ratios, obtained from their own data products, to the observed ET values for each watershed. The importance of deriving PET values for each data product through this rescaling approach (referred to rescaled PET), rather than using the original PET product, is to ensure consistency between the PET values and the observed ET values for each watershed while preserving the ET/PET ratios from the individual products. This is necessary not least because the magnitudes of some original PET products are smaller than their corresponding observed ET values.

In essence, we derive new PET values for all six products using Equation (9), maintaining the ET/PET ratio for each data product (except for GLEAM). This approach yields consistent PET values across the six datasets while capturing the essential variations among them. The rescaled PET values obtained from Equation (9) uphold the fundamental principles of individual

175 products by preserving their respective ET/PET ratios. By doing so, the effects stemming from differences or uncertainties in their inputs/forcing data are notably mitigated, as the new PET values are calculated using observed ET and their own ET/PET ratios. This concept is akin to the notion of emergent constraints employed by others (Green et al., 2024; Hall et al., 2019; Williamson et al., 2021):

$$PET_{rescaled} = \frac{PET_{dataset}}{ET_{dataset}} \times ET_{obs} \qquad\qquad 1. \quad (9)$$

where $ET_{dataset}$ and $PET_{dataset}$ are values extracted from different data products, and ET_{obs} is observed ET calculated as $P -$
180 Q based on observed P and Q for each watershed. Table 3 shows the correlation between the rescaled PET values of the six data products; the correlations show good consistency between the rescaled PET values. These six rescaled PET data products are then applied to Equations 2-5 to obtain T/ET ratios for each of the six vegetation types over the 648 watersheds. With the six rescaled PET data products, we can assess how variations in PET affect the robustness of our new method in estimating T/ET.

185

Figure 2: Original PET for six data products: NARR, MODIS, Zhang, GLEAM v3.5a, SPLASH, and BESS v2 for 648 watersheds. (a) PET values retrieved from the data products, and (b) ET/PET ratios retrieved from the data products. Watersheds are sorted in descending order according to GLEAM's ET/PET.

Table 3: Correlations between rescaled PET of six data products: NARR, MODIS, Zhang, GLEAM v3.5a, SPLASH, and BESS v2
190 **for 648 watersheds.**

	MODIS	*GLEAM*	*NARR*	*SPLASH*	*BESS*	*Zhang*
MODIS	1					
GLEAM v3.5a	0.72	1				
NARR	0.81	0.83	1			
SPLASH	0.80	0.84	0.83	1		
BESS	0.92	0.78	0.73	0.75	1	

9

Zhang	0.70	0.83	0.68	0.69	0.92	1

4 Results

Figure 3 shows the estimated values of λ for each of the six datasets based on Equations 6-8. Figure 4 shows the comparison between observed soil wetting (W) and the simulated soil wetting with estimated λ value for a representative vegetation type. The six datasets show similar trends, where the highest λ values are observed for the shrubs and grass vegetation types. Crops have lower λ values than shrubs and grass, but equal or higher than those for forests according to the dataset used. Figure 3 illustrates that the greatest variations among the six data products occur in the mixed forest and crops. This discrepancy may be attributed to differences in how each data product defines mixed forest and crop compositions, resulting in varying estimated parameters.
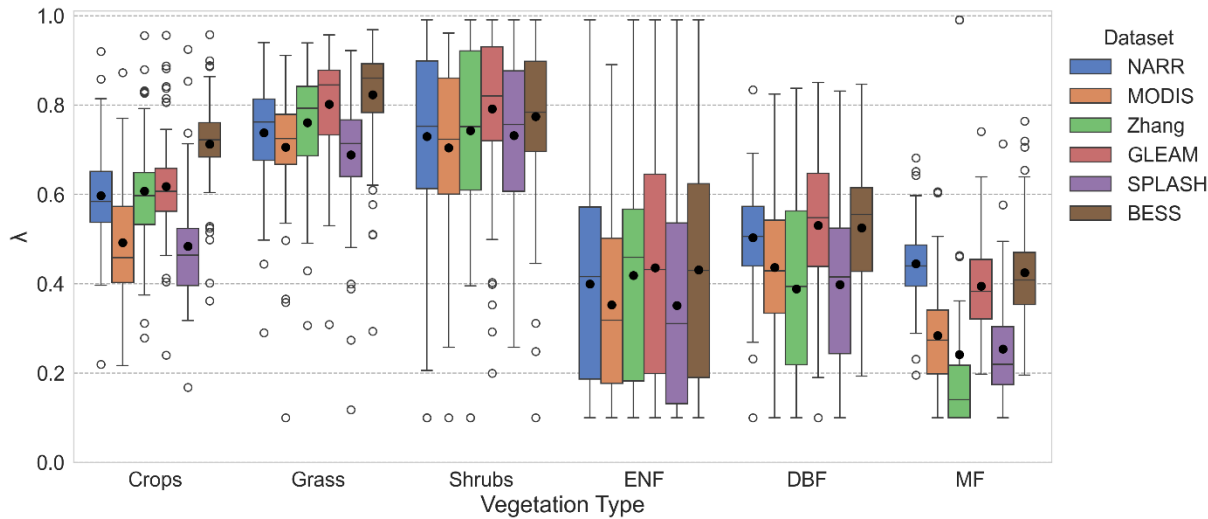

Figure 3: λ values for the watersheds using data from six datasets: NARR, MODIS, Zhang et al. (2010), GLEAM after rescaling, SPLASH, and BESS. Note that ENF, DBF, and MF represent, respectively, evergreen needle-leaf forest, deciduous broadleaf forest, and mixed forest in the figure.
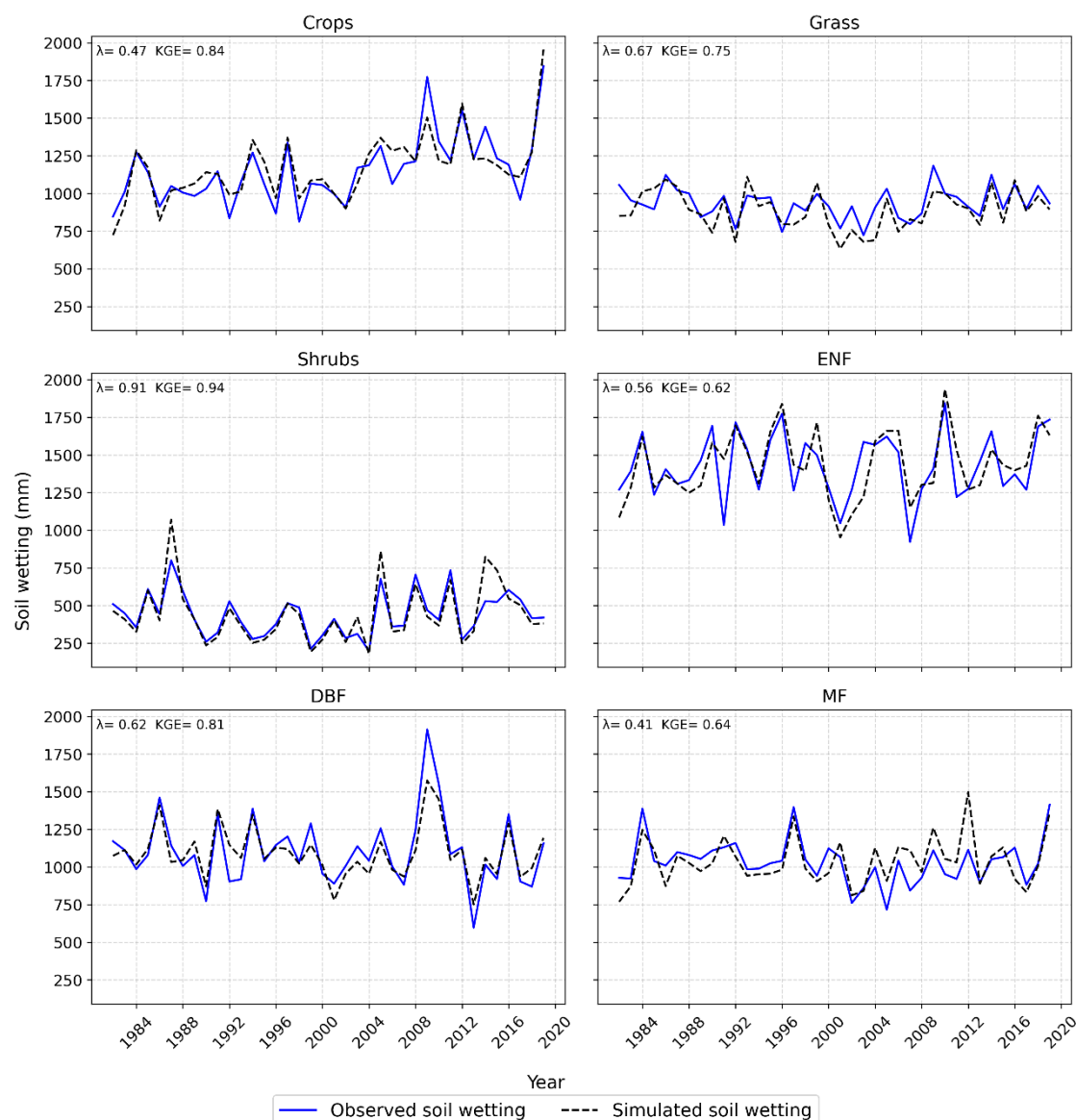
Figure 4: Optimization of λ values using observed and simulated soil wetting as explained in equations 6-8. Figure shows observed
205 **and simulated soil wetting time series for an example watershed for each of the six vegetation types (crops, grass, shrubs, ENF, DBF, MF).**

T/ET ratios are shown in Figure 5 and Table 4. Overall, the trend is consistent among the six datasets. Grass and shrubs have the lowest T/ET values, with mean T/ET in the range of 0.19-0.39. Crops have higher mean T/ET ratios, with NARR, Zhang, and GLEAM averaging around 0.4, while MODIS and SPLASH show a higher crop mean T/ET of around 0.51. BESS has the
210 lowest crop T/ET with a value of 0.29. All datasets have similar forest T/ET trend, with lowest mean T/ET for DBF (0.46-0.60), followed by ENF (0.52-0.71). The highest mean T/ET is exhibited for MF (0.55-0.76).
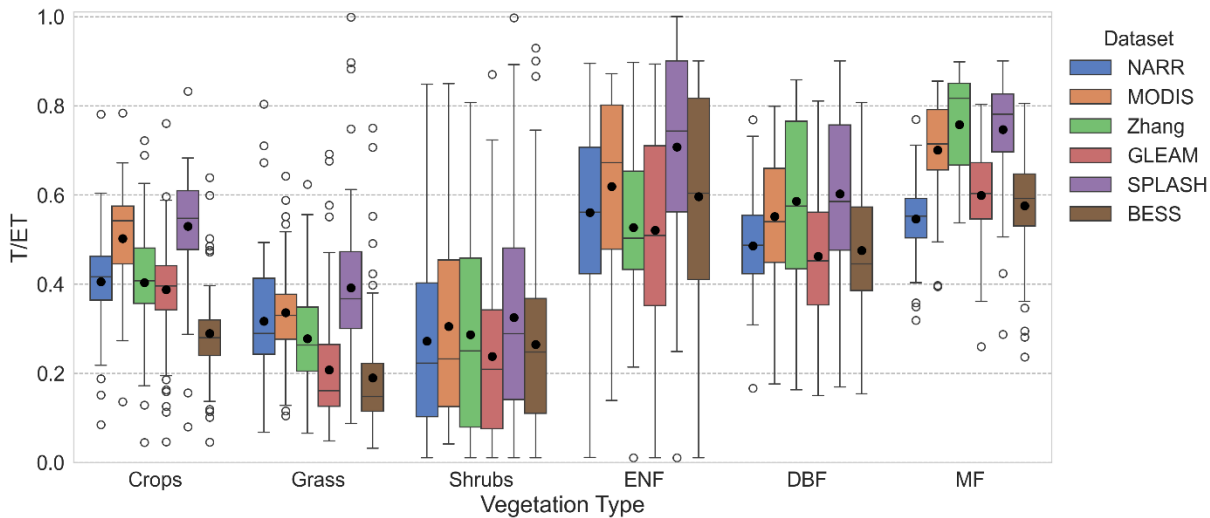
11

Figure 5: T/ET values for the watersheds using data from the six datasets: NARR, MODIS, Zhang et al. (2010), GLEAM after rescaling, SPLASH, and BESS

215 **Table 4: Mean T/ET values for six vegetation types using PET data from the six data products. Minimum, maximum, and mean values are shown for each vegetation type.**

Data product	Crops	Grass	Shrubs	ENF	DBF	MF	Mean
NARR	0.42	0.35	0.40	0.71	0.51	0.55	0.49
MODIS	0.54	0.40	0.44	0.79	0.58	0.72	0.58
Zhang	0.41	0.31	0.36	0.72	0.63	0.79	0.54
GLEAM	0.40	0.22	0.30	0.65	0.48	0.61	0.44
SPLASH	0.54	0.41	0.40	0.78	0.63	0.74	0.58
BESS	0.42	0.28	0.36	0.70	0.49	0.66	0.49
Minimum	**0.40**	**0.22**	**0.30**	**0.65**	**0.48**	**0.55**	**0.44**
Maximum	**0.54**	**0.41**	**0.44**	**0.79**	**0.63**	**0.79**	**0.58**
Mean	**0.46**	**0.33**	**0.38**	**0.73**	**0.55**	**0.68**	**0.52**

5 Discussion

5.1 λ and T/ET ratios

220 Shrubs and grass showed higher λ values, likely due to their occurrence in arid and semi-arid regions in the US. The high λ values could be explained by the higher bare soil evaporation expected in arid regions (Baver et al., 1972), especially due to

the sparse nature of shrubs, increasing bare areas and thus bare soil evaporation (Liu et al., 2022). Also, the high aridity is expected to cause water stress, lowering the continuing transpiration (portion of transpiration not included in λ). The lower λ values in crops and forests may be due to the higher vegetation coverage in these areas which provides shade to the soil,

225 reducing the amount of soil evaporation (Baver et al., 1972). Additionally, litter contributes to reducing soil evaporation, and may even have a larger reducing effect than canopy shade (Magliano et al., 2017). The broader leaves of DBF increase their interception compared to ENF, thus resulting in a higher λ value as well.

These estimated mean T/ET ratios followed explainable trends, with shrubs and grass watersheds showing low T/ET ratios, forests exhibiting higher T/ET ratios, and crops falling in between. Given greater water availability in crops and forests, it is

230 expected that they would exhibit higher T/ET ratios. Many crops in the US benefit from continuous irrigation, reducing water stress and promoting transpiration. Forests, with their dense canopy cover offering shade, reduce soil evaporation (Baver et al., 1972) and consequently boost the T/ET ratios. Crops also show high vegetation coverage, thereby providing shade to the soil and increasing T/ET (Baver et al., 1972). Moreover, in arid regions dominated by shrubs, lower soil water content is anticipated, resulting in diminished root water uptake (Gardner, 1983). Furthermore, the shedding of leaves in deciduous

235 forests reduces transpiration when examined over the whole year (as here), resulting in a decreased T/ET ratio for DBF.

Differences in study scale may hinder the comparison with other studies, since our method estimates T/ET at the watershed scale, while other studies are based at a plot-scale (field/eddy covariance-based methods) or grid scale (models and remote-sensing methods). Factors affecting watershed scale T/ET include the possible presence of secondary vegetation within the watershed and the possible sparseness of the primary vegetation and presence of bare areas which can increase soil evaporation

240 and reduce T/ET, especially for shrublands. Therefore, this method has the advantage of providing a realistic watershed T/ET ratio that accounts for multiple vegetation types and sparseness in vegetation distribution. Consistent results across different datasets underscore the reliability of our new method, irrespective of the data product employed (see Fig. 5 and Table 3).

5.2 Effect of hydrological indices on T/ET

We explore the sensitivity of T/ET to two hydrological indices, namely the runoff ratio (Q/P) and the baseflow ratio (Q_b/Q).

245 Figure 6a shows a proportional relationship between T/ET and Q/P. The relationship appears to manifest as two distinct linear correlations, with arid catchments showing a steeper slope than humid catchments. Arid regions typically experience minimum runoff as a significant portion of precipitation evaporates in various forms owing to elevated atmospheric demand. This phenomenon yields high T/ET ratios at relatively low Q/P values. Conversely, humid catchments often experience substantial runoff, attributed to either saturation excess or infiltration excess runoff mechanisms, resulting in elevated Q/P ratios compared

250 to arid catchments at equivalent T/ET values. In both cases, a higher Q/P ratio signifies increased water availability, consequently leading to higher T/ET ratios.

In Figure **6**b a non-linear positive relationship is depicted between the mean T/ET and Qb/Q (baseflow ratio). The baseflow ratio serves as an indicator of soil water availability, as higher baseflow typically corresponds to increased soil moisture content (Hurkmans et al., 2008). Consequently, a positive correlation between T/ET and the baseflow ratio is anticipated. Notably, the

255 majority of arid catchments cluster in the low Qb/Q and low T/ET region, while transitioning toward wetter catchments naturally augments both Qb/Q and T/ET.
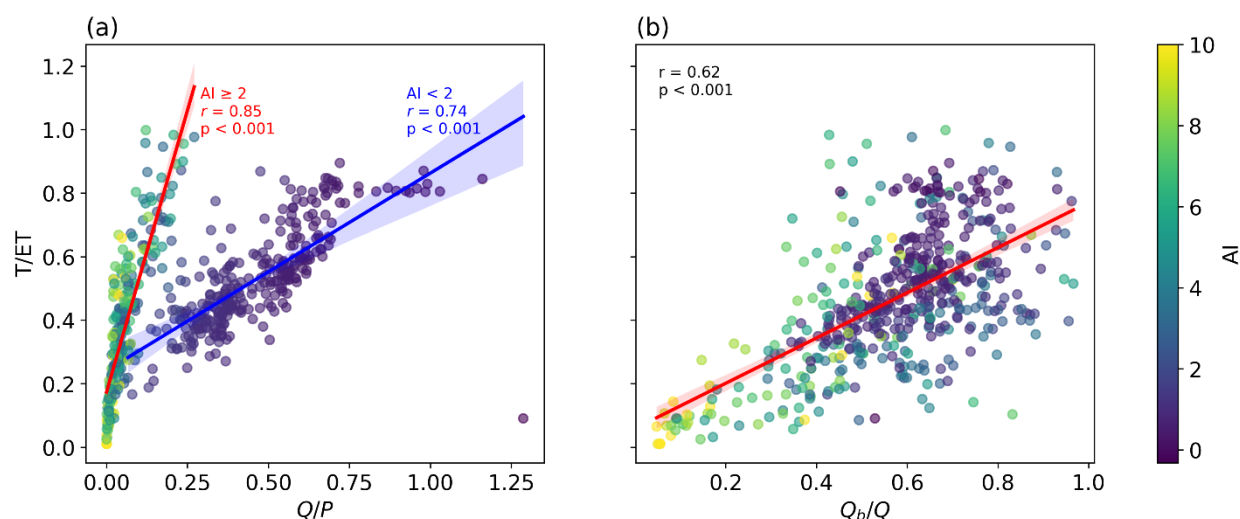
2.

Figure 6: Relationship between mean T/ET and two hydrological indices (a) Q/P and (b) Qb/Q for 648 watersheds based on NARR
260 **data. Plots are colored according to aridity index.**

5.3 Effect of LAI on T/ET

The leaf area index (LAI), representing the leaf area per unit ground area, reflects the combined influences of leaf size and canopy density. As shown in Figure **7**, LAI appears to exert some influence over ET partitioning. Arid watersheds show lower LAI values, and T/ET ratios increase non-linearly with LAI. However, as watersheds transition toward higher humidity levels,
265 their LAI and T/ET ratios increase non-linearly, albeit at different rates. In arid regions, plants tend to reduce their leaf area to mitigate water loss (Chaves et al., 2003), thereby decreasing both LAI and T/ET – a direct consequence of heightened aridity. This suggests that aridity plays a role in regulating T/ET. Conversely, Figure **7** illustrates a complex relationship between LAI and T/ET, characterized by substantial scatter. Our findings align with previous studies indicating diverse dependence of T/ET on LAI. For instance, LAI has been shown to provide a control on ET partitioning (Li et al., 2019; Wang et al., 2014; Wei et
270 al., 2017), but that effect varies from one study to another. Wang et al. (2014) showed that LAI has a non-linear relationship with T/ET during the growing season, whereas Li et al. (2019) showed a weak linear relationship between mean growing season LAI and mean annual T/ET across sites, with the T/ET and LAI relationship within the same site being non-linear. Additionally, Cao et al. (2022) showed a non-linear positive relationship between annual T/ET and LAI.

14
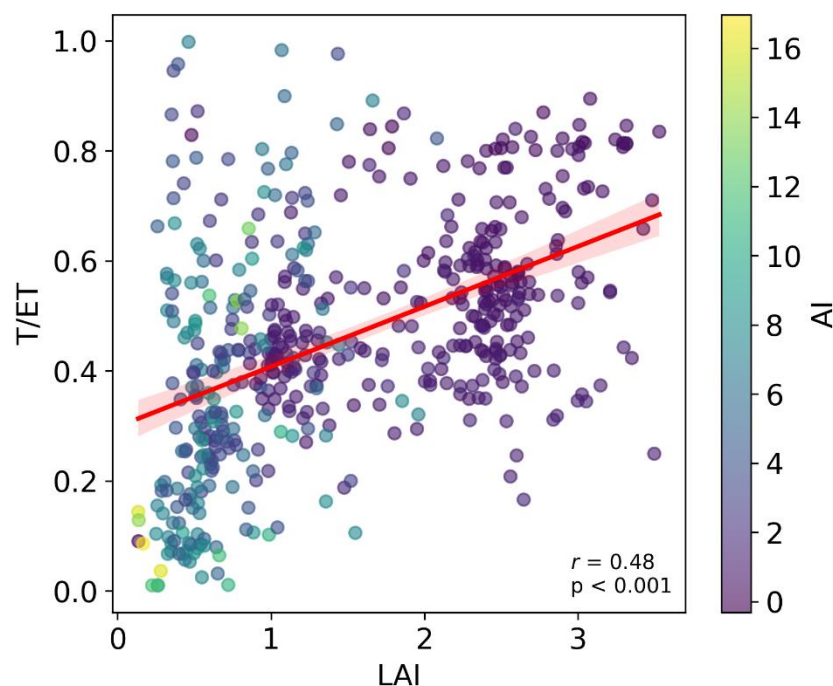
Figure 7: Relationship between T/ET and LAI for 648 watersheds using T/ET calculated based on the NARR dataset.

5.4 Impacts of environmental variables on T/ET ratios

We explore the effect six environmental factors on the mean T/ET ratios. They are aridity index (AI), relative humidity (RH), air temperature (T_{air}), downward shortwave radiation (DSW), soil moisture, and wind speed (WS). These factors were derived from the NARR dataset, and the T/ET ratios were calculated based on the same dataset. Since some of these environmental variables are highly correlated (as shown in Figure 8), we first perform variable selection using stepwise regression and Lasso regression to identify those that are strongly correlated with each other. Stepwise regression aims to select a subset of variables that provide the best prediction with minimum redundancy, while Lasso regression adds a penalty term to reduce the coefficients of insignificant variables. Both methods resulted in the elimination of relative humidity and downward shortwave radiation. Table 5 shows the coefficients of the environmental variables and their significance for both stepwise and Lasso regression. Although the significance test shows that air temperature has an insignificant impact, while the aridity index, soil moisture, and wind speed are significant (Table 5), air temperature is still included because it marginally contributes to the model's predictive power. Additionally, it represents an independent and observable dimension, distinct from the other three significant environmental variables.

A negative non-linear correlation between T/ET and AI is present. Increased aridity prompts plants to adopt water conserving strategies (Chaves et al., 2003), thereby reducing the transpiration ratios. In humid regions, the relationship between T/ET and AI is more discernible, with AI accounting for a significant portion of the variance of T/ET. Conversely, for arid regions,

15

particularly those dominated by shrubs, the relationship shows greater scatter, suggesting that AI exerts a relatively smaller effect on T/ET, while other factors play a more prominent role. Furthermore, higher air temperature contributes to lowering T/ET (see Fig. 9b), as it prompts water-conserving behaviors in plants and elevates soil evaporation, consequently reducing

295 T/ET ratios. Conversely, increasing soil moisture leads to enhanced water availability for plant root uptake, resulting in a near linear increase in T/ET, as shown in Figure 9c. The relationship between wind speed (WS) and T/ET is inconclusive; this finding is consistent with several previous studies (e.g., Dixon and Grace, 1984; Huang et al., 2015; Schymanski and Or, 2016), which have presented a mixed effect of wind speed on transpiration. Nevertheless, the effects of other environmental variables on T/ET demonstrate explainable patterns as discussed here. The other five data products (MODIS, Zhang, GLEAM, SPLASH,

300 and BESS) show similar impacts of all the environmental variables on T/ET as those shown in Figure **9** for NARR.
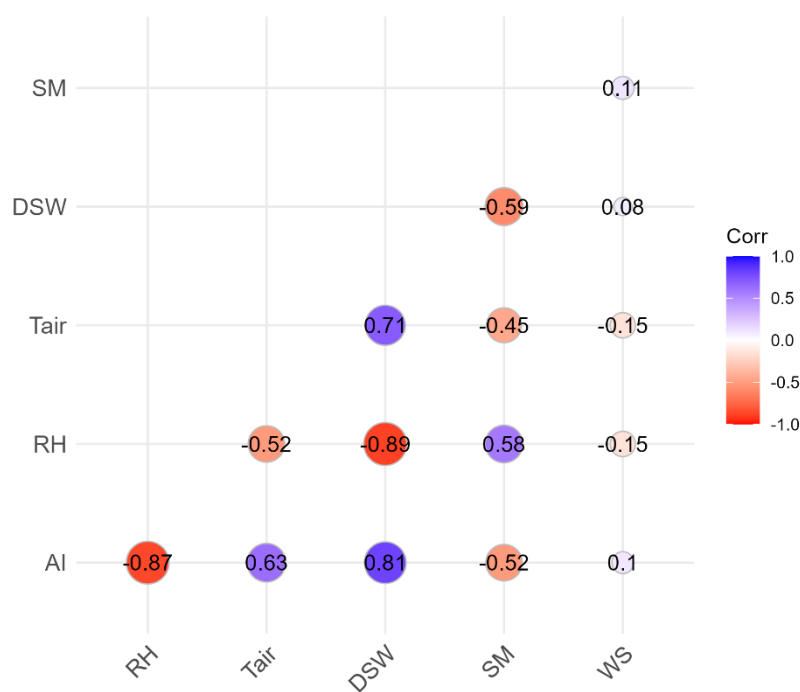

Figure 8: Correlation between environmental variables. AI: aridity index, RH: relative humidity, Ta: air temperature, DSW: downward shortwave radiation, SM: soil moisture, WS: wind speed.

Table 5: Coefficients of standardized environmental variables regressed against T/ET using stepwise selection and Lasso regression.
305 **Significance levels are shown next to the coefficients (***: $p<0.001$, **: $p<0.01$, *: $p<0.05$, blank: $p>0.1$**

	Coefficient (Stepwise selection)	Coefficient (Lasso regression)
AI	-0.065***	-0.022***
RH		
Tair	-0.015	-0.003

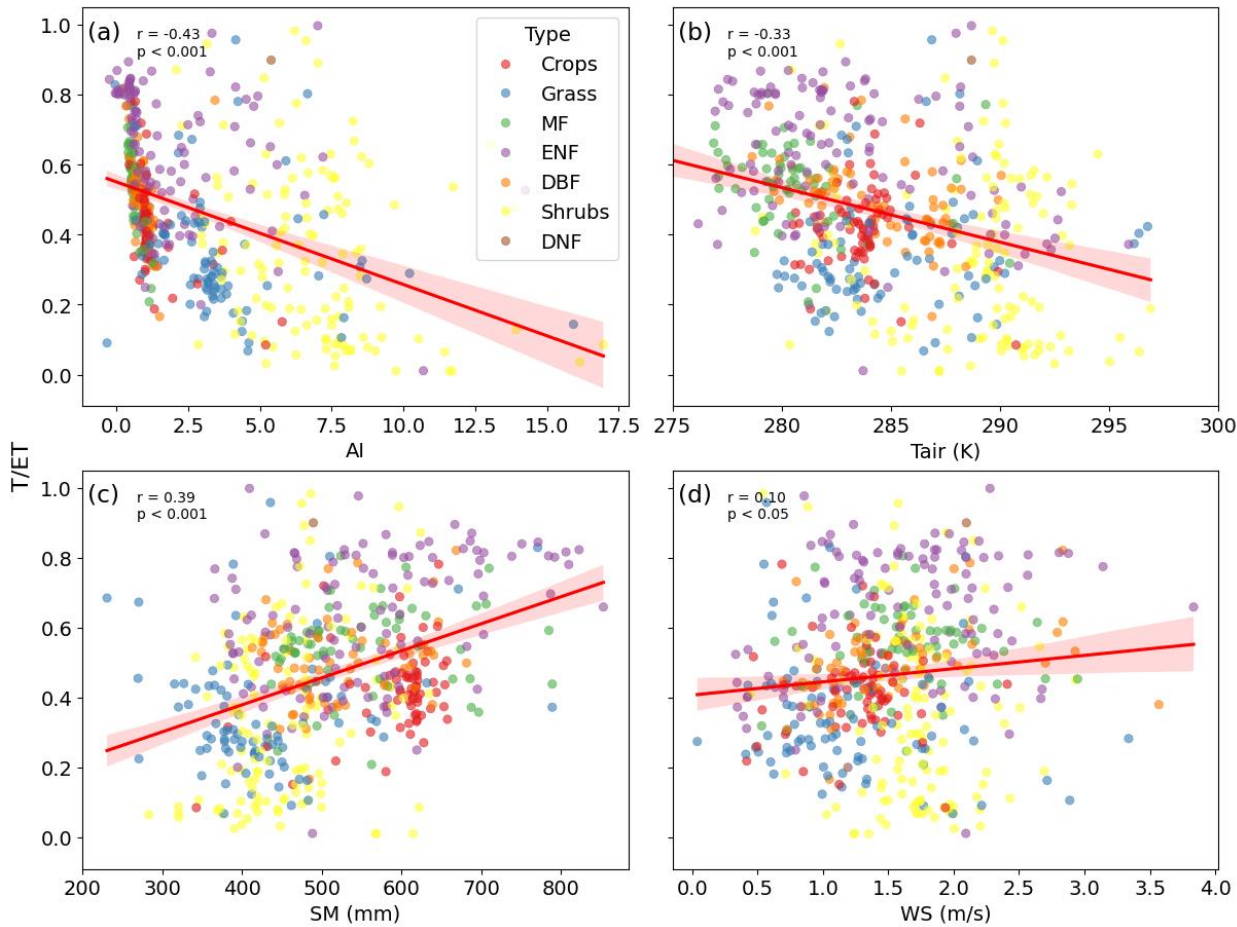| DSW		
SM	0.039***	0.0003***
WS	0.025**	0.042**

Figure 9: Relationships between mean annual T/ET and environmental factors (a) aridity index (PET/P), (b) air temperature (Tair), (c) soil moisture (SM), and (d) wind speed (WS) for 648 watersheds. T/ET is calculated based on NARR data, and the environmental variables are also retrieved from the NARR product. Significance of the pairwise relationships between T/ET and the environmental variables are shown on each plot.

5.5 T/P ratios

We computed transpiration to precipitation (T/P) ratios based on T/ET values calculated from the six adjusted PET data products. The mean T/P ratios from these six datasets range from 0.24 to 0.36, aligning closely with the global mean T/P of 0.39 estimated by Schlesinger and Jasechko (2014).

We also compared our estimated T/P ratios to the T/P versus aridity index relationship identified by Good et al. (2017). Good et al. (2017) presented this relationship based on a compilation of field studies, three remote-sensing based models, and an ecohydrological model, revealing good consistency among the various T/P data sources. Figure 10 shows a similar trend to that presented in Fig. 1 of Good et al. (2017), with the maximum T/P ratio close to the intersection between water and energy-

320   limited states. This maximum T/P corresponds to an aridity index ranging between 2 and 3 in our study, similar to the estimated aridity index range of 1.3 to 1.9 for the maximum T/P as reported by Good et al. (2017). Moreover, the maximum T/P shown in Figure **10** ranges between 0.5 and 0.58, consistent with the maximum T/P of 0.6 based on field data in Good et al. (2017). Notably, there is greater variation on the right side of the curve (indicating more arid conditions) compared to the left side (representing wetter conditions). In arid regions, transpiration is influenced not only by aridity, but also by factors such as

325   groundwater table depth and soil moisture content, resulting in higher variability in the T/P versus aridity index (AI) relationship. The consistency between Good et al. (2017) and this study suggests that this relationship holds not only at the field scale (as shown by Good et al., 2017), but also at the watershed scale, as demonstrated in this study. This relationship holds significance for studies like that of Cai et al. (2023), where T/P serves as a parameter (referred to as f_0 in their study) to determine water-limited fAPAR and LAI. Currently, in their study, this T/P ratio is estimated as a global mean using non-

330   linear regression, with a value of 0.62, akin to the maximum T/P of 0.5 to 0.58 estimated by our fitted curves depicted in Figure **10**. Utilizing a variable T/P as a function of AI, as demonstrated by the derived relationships here, could prove beneficial in improving fAPAR and LAI estimates on a global scale.

18
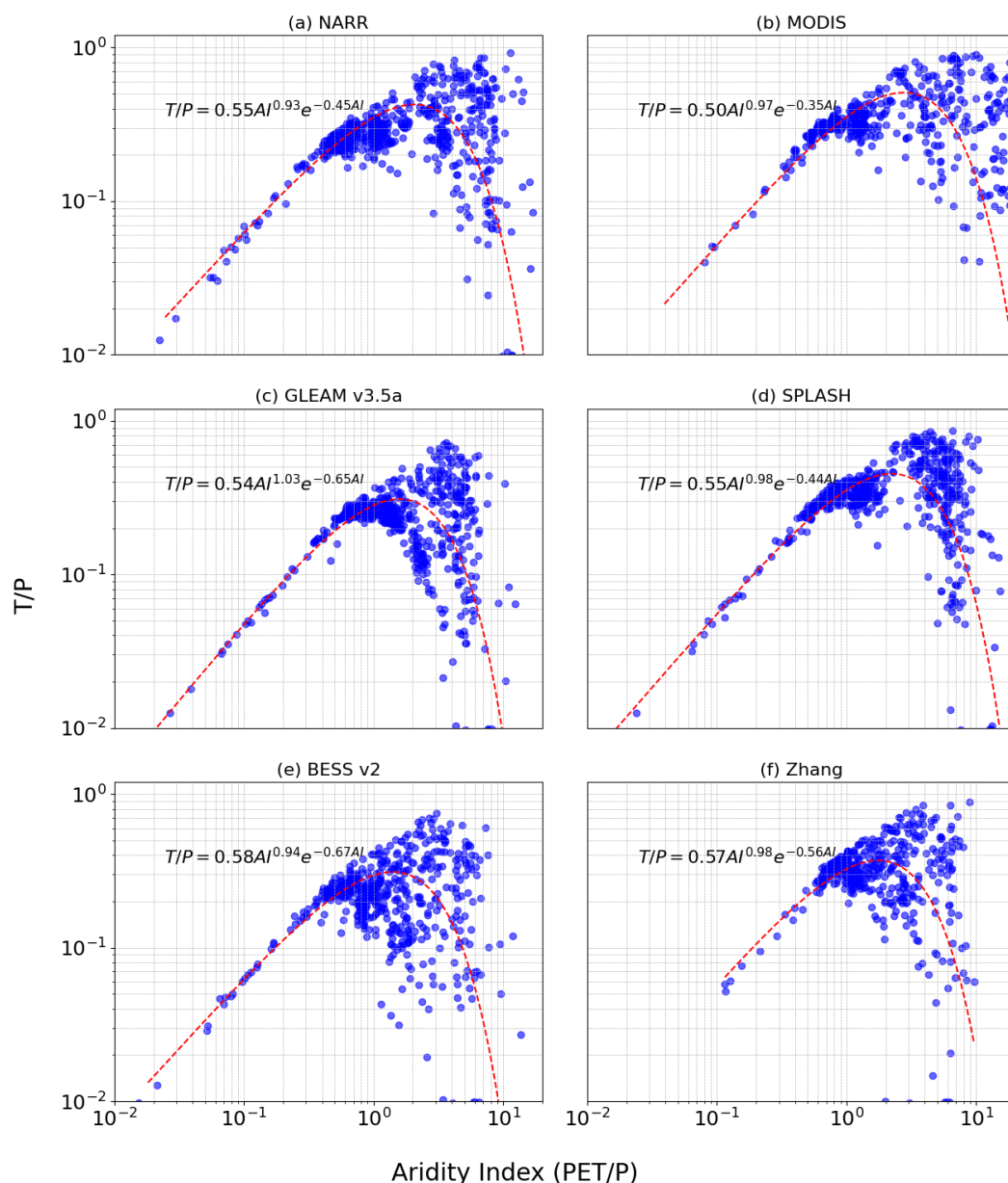
Figure 10: T/P versus the aridity index for six datasets: (a) NARR, (b) MODIS, (c) Zhang et al. (2010), (d) GLEAM after rescaling, (e) SPLASH, (f) BESS

6 Variation of ET partitioning methods

Figure 5 demonstrates the influence of the six adjusted PET data products on the T/ET ratios by our new method for each vegetation type, while Table 4 provides their variation range between the minimum and maximum mean T/ET ratios. On the

340   other hand, as outlined in the introduction, estimated global mean values of T/ET from various existing methods exhibit a

       considerable variation, ranging from 0.24 to 0.9 (Liu et al., 2022; Wei et al., 2017). This variation may be attributed to several

       factors, including data inconsistencies, geographical disparities, and differences in selected time periods, apart from differences

       in methodology. In an effort to explore what may be the cause for the large variation among the different methods, we have

       tried to mitigate these factors by using the same half-hourly eddy covariance data from the FLUXNET and AMERIFLUX

345   ONEFLUX towers measurements in the US for the same locations and same time periods. Such an approach would allow us

       to elucidate the disparities among the existing ET partitioning methods, consequently, providing insights on influences by

       different PET datasets in our method versus current existing different methods on the large range of T/ET ratios.

       The four methods we selected to investigate are: (1) Zhou et al. (2016), (2) Scott and Biederman (2017), (3) Li et al. (2019),

       and (4) Yu et al. (2022). These four methods are selected because they are based on eddy covariance measurements whose

350   data are widely available, unlike sap flow and isotope measurements. Since these methods are based on flux measurements,

       they can be considered as field-based estimations of T/ET. We apply these four methods to the same datasets from the

       FLUXNET and AMERIFLUX ONEFLUX towers in the US, but the final number of flux towers included for each method

       depends on the filtering criteria in each method and the limitations in applying each method.

       The first method by Zhou et al. (2016) is based on the water use efficiency. The ratio T/ET is estimated as the ratio between

355   the apparent water use efficiency ($WUE_a = GPP \times \frac{VPD^{0.5}}{ET}$) and the potential water use efficiency ($WUE_p = GPP \times \frac{VPD^{0.5}}{T}$).

       Assuming that T/ET approaches 1 at some time during the growing season, the WUE_p is estimated from the 95th quantile

       regression of the half-hourly scatter plot (based on all half-hourly data for the site) between GPP×VPD$^{0.5}$ and ET and is

       assumed to be constant for the flux tower. WUE_a is then estimated for each time step as the linear regression of the ET and

       GPP×VPD$^{0.5}$ relationship using half-hourly data for the desired time period, which can be 8-day, monthly or annually.

360   The second method by Scott and Biederman (2017) is based on water use efficiency to estimate multiyear monthly average

       T/ET ratios. This approach estimates transpiration as the product of the inverse of the marginal water use efficiency, the ratio

       between transpiration WUE and marginal WUE, and GPP. The inverse of the marginal WUE is estimated from the linear

       regression of the GPP versus ET scatter plot. The ratio between transpirational and marginal WUEs is assumed to be 1. This

       method requires multiple years of data for its application.

365   The third method by Li et al. (2019) is based on the stomatal conductance model of Lin et al. (2018) to partition ET. The T/ET

       ratio is equivalent to the ratio between canopy conductance and ecosystem conductance. The eddy covariance data are divided

       into soil moisture bins to calibrate the parameters. Therefore, the method requires soil moisture data, along with GPP, VPD,

       ET, and three calibrated parameters to estimate the T/ET ratio.

       The fourth method by Yu et al. (2022) combines the water use efficiency with the Medlyn et al. (2011) stomatal conductance

370   model. This method relies on GPP, ET, C_a, P_a, and VPD from the flux tower data in addition to the parameter g_1 from the

       Medlyn et al. (2011) model. The authors compared their method to other methods and showed a high correlation with the Zhou

       et al. (2016) but a low correlation with the Li et al. (2019) method.

Additionally, we compare our results to T/ET values for 20 global flux towers from Tan et al. (2021). T/ET was calculated based on flux tower data and P-model (Stocker et al., 2020; Wang et al., 2017) outputs.

375   The estimated T/ET ratios from the five methods are shown in Figure 11a – e and Table 4, respectively, for the same six different vegetation types as shown in Figure **5** with our new method.
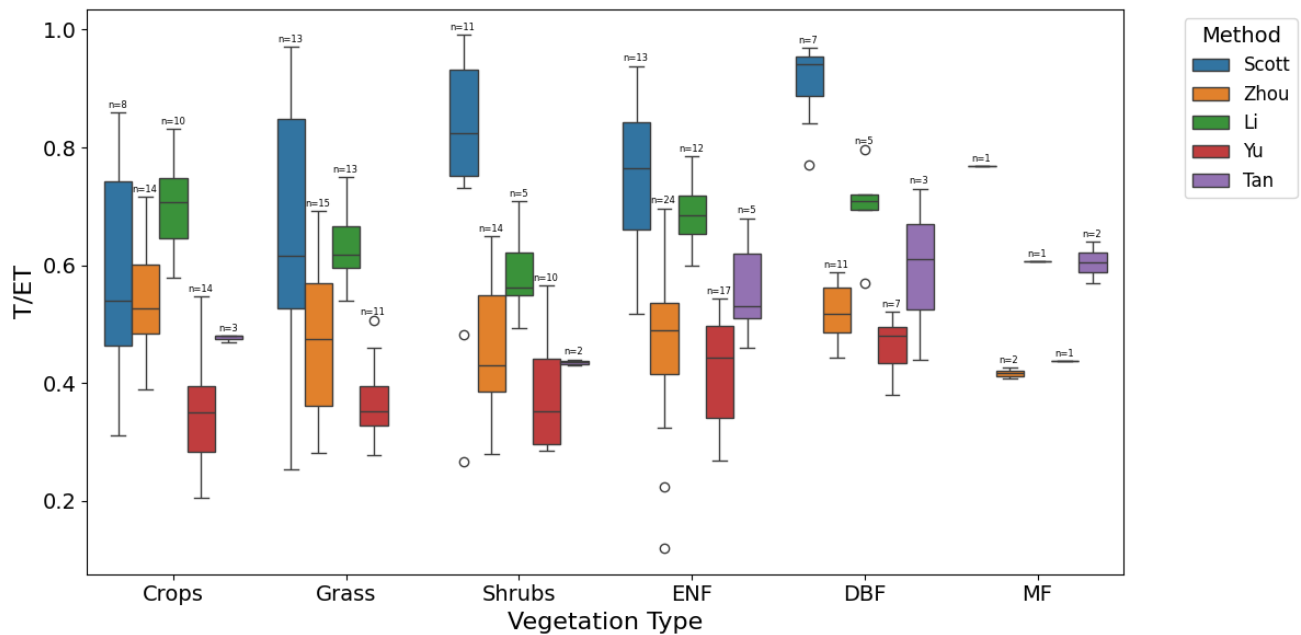
Figure 11: T/ET values based on the eddy covariance tower data with 5 methods: (a) Zhou et al. (2016) (n=8480), (b) Scott and Biederman (2017) (n=53), (c) Li et al. (2019) (n=46), (d) Yu et al. (2022) (n=60) (e) Tan et al. (2021) (n=15).

Table 6: Mean T/ET values for six vegetation types using four ET partitioning methods. Minimum, maximum, and mean values are shown for each vegetation type.

ET partitioning method	Crops	Grass	Shrubs	ENF	DBF	MF	Mean
Zhou et al.	0.54	0.48	0.46	0.46	0.52	0.42	0.48
Scott and Biederman	0.56	0.59	0.65	0.66	0.65	0.77	0.62
Li et al.	0.70	0.63	0.59	0.69	0.70	0.61	0.66
Yu et al.	0.34	0.37	0.38	0.43	0.46	0.44	0.39
Tan et al.	0.48	-	0.44	0.56	0.6	0.61	0.54
Minimum	**0.34**	**0.37**	**0.38**	**0.43**	**0.46**	**0.42**	**0.39**

| Maximum | 0.70 | 0.63 | 0.65 | 0.69 | 0.70 | 0.77 | 0.66 |
| Mean | 0.52 | 0.52 | 0.50 | 0.56 | 0.59 | 0.57 | 0.54 |

The inconsistencies among the five methods are evident, with Zhou, Yu, Li, and Tan showing minimal variation among vegetation types, while Scott displays substantial variation. Moreover, the magnitudes and trends of T/ET across these methods are also inconsistent. These discrepancies indicate a lack of agreement on both the mean T/ET values and the variation ranges among the different methods. Consequently, these methods are not suitable as reference points for evaluating our new method. Instead, the assessment of our new method should be based on its physical behavior and relationships with other variables, as discussed in Section 5. It is noteworthy that compared to Figure **5**, the variation range of T/ET ratios from the five different methods, utilizing the same data at the same locations, is significantly greater than that for our new method in which disparity is attributed to the variations associated with the PET methods employed.

7 Conclusions

We have presented a new method for determining the transpiration to total evapotranspiration (T/ET) ratio using long-term hydrological observations. This method is based on the generalized proportionality hypothesis, which has wide applications in hydrology. We applied the method to 648 watersheds in the US using six different PET data products. Our findings demonstrate consistent T/ET results across these diverse PET datasets, facilitated by a rescaling of PET derived from the ET/PET ratios obtained from each data product and observed ET computed from the watershed water balances.

Our analysis reveals that varying T/ET ratios across watersheds are associated with different vegetation types, with shrubs and grasslands exhibiting lower T/ET values compared to crops and forests. Furthermore, our results underscore the significant influence of leaf area index (LAI), hydrological indices (Q/P and Qb/Q), and prevailing environmental conditions on T/ET. Our method also provides a realistic estimate of T/ET at a watershed scale that implicitly accounts for the heterogeneity of vegetation within the catchment. Our method can also be useful for constraining hydrological models, land surface models, and climate models.

We also explore the relationship between T/ET and aridity index, unveiling a bell-shaped curve at the watershed scale, where the maximum T/ET ratio occurs at an aridity index between 2 and 3, corresponding to a T/P ratio of around 0.5 to 0.58. These findings provide valuable insights into the intricate interplay between hydrological processes and environmental variables, shedding light on the complex dynamics of evapotranspiration in diverse watershed ecosystems.

Acknowledgements

Author contributions: AH implemented the research ideas, designed and performed the experiments, analyzed the results, drafted the manuscript. XL conceived the research ideas, designed the experiments, analyzed the results, supervised the investigation, and wrote and finalized the manuscript. ICP initiated the research topic, analyzed the results, edited the
415 manuscript.

Competing interests: The authors declare that they have no conflict of interest.

References

420 Abeshu, G.W., Li, H.Y., 2021. Horton Index: Conceptual Framework for Exploring Multi-Scale Links Between Catchment Water Balance and Vegetation Dynamics. Water Resour Res 57. https://doi.org/10.1029/2020WR029343

Alemohammad, S.H., Fang, B., Konings, A.G., Aires, F., Green, J.K., Kolassa, J., Miralles, D., Prigent, C., Gentine, P., 2017. Water, Energy, and Carbon with Artificial Neural Networks (WECANN): A statistically based estimate of global surface turbulent fluxes and gross primary productivity using solar-induced fluorescence. Biogeosciences 14, 4101–4124.
425 https://doi.org/10.5194/BG-14-4101-2017

Arsenault, R., Brissette, F., Martel, J.L., Troin, M., Lévesque, G., Davidson-Chaput, J., Gonzalez, M.C., Ameli, A., Poulin, A., 2020. A comprehensive, multisource database for hydrometeorological modeling of 14,425 North American watersheds. Sci Data 7. https://doi.org/10.1038/s41597-020-00583-2

Baver, L.D., Gardner, W.H., Gardner, W.R., 1972. Soil Physics. John Wiley & Sons, New York.

430 Berkelhammer, M., Noone, D.C., Wong, T.E., Burns, S.P., Knowles, J.F., Kaushik, A., Blanken, P.D., Williams, M.W., 2016. Convergent approaches to determine an ecosystem's transpiration fraction. Global Biogeochem Cycles 30, 933–951. https://doi.org/10.1002/2016GB005392

Cai, W., Zhu, Z., Harrison, S.P., Ryu, Y., Wang, H., Zhou, B., Prentice, I.C., 2023. A unifying principle for global greenness patterns and trends. bioRxiv 2023.02.25.529932. https://doi.org/10.1101/2023.02.25.529932

435 Cao, R., Huang, H., Wu, G., Han, D., Jiang, Z., Di, K., Hu, Z., 2022. Spatiotemporal variations in the ratio of transpiration to evapotranspiration and its controlling factors across terrestrial biomes. Agric For Meteorol 321. https://doi.org/10.1016/j.agrformet.2022.108984

Cavanaugh, M.L., Kurc, S.A., Scott, R.L., 2011. Evapotranspiration partitioning in semiarid shrubland ecosystems: a two-site evaluation of soil moisture control on transpiration. Ecohydrology 4, 671–681. https://doi.org/10.1002/ECO.157

440 Čermák, J., Deml, M., Penka, M., 1973. A new method of sap flow rate determination in trees. Biol Plant 15, 171–178. https://doi.org/10.1007/BF02922390

Čermák, J., Kučera, J., Nadezhdina, N., 2004. Sap flow measurements with some thermodynamic methods, flow integration within trees and scaling up from sample trees to entire forest stands. Trees 2004 18:5 18, 529–546. https://doi.org/10.1007/S00468-004-0339-6

445   Chaves, M.M., Maroco, J.P., Pereira, J.S., 2003. Understanding plant responses to drought — from genes to the whole plant. Functional Plant Biology 30, 239. https://doi.org/10.1071/FP02076

Cohen, Y., Fuchs, M., Green, G.C., 1981. Improvement of the heat pulse method for determining sap flow in trees. Plant Cell Environ 4, 391–397. https://doi.org/10.1111/J.1365-3040.1981.TB02117.X

Damm, A., Roethlin, S., Fritsche, L., 2018. Towards advanced retrievals of plant transpiration using suninduced chlorophyll

450   fluorescence: First considerations. International Geoscience and Remote Sensing Symposium (IGARSS) 2018-July, 5983–5986. https://doi.org/10.1109/IGARSS.2018.8518974

Davis, T.W., Prentice, I.C., Stocker, B.D., Thomas, R.T., Whitley, R.J., Wang, H., Evans, B.J., Gallego-Sala, A. V., Sykes, M.T., Cramer, W., 2017. Simple process-led algorithms for simulating habitats (SPLASH v.1.0): Robust indices of radiation, evapotranspiration and plant-available moisture. Geosci Model Dev 10, 689–708. https://doi.org/10.5194/GMD-10-689-2017

455   Dixon, M., Grace, J., 1984. Effect of Wind on the Transpiration of Young Trees. Ann Bot 53, 811–819. https://doi.org/10.1093/oxfordjournals.aob.a086751

Fan, J., McConkey, B., Wang, H., Janzen, H., 2016. Root distribution by depth for temperate agricultural crops. Field Crops Res 189, 68–74. https://doi.org/10.1016/j.fcr.2016.02.013

Gardner, W.R., 1983. Soil Properties and Efficient Water Use: An Overview. pp. 45–64.

460   https://doi.org/10.2134/1983.limitationstoefficientwateruse.c3

Gerrits, A.M.J., Savenije, H.H.G., Veling, E.J.M., Pfister, L., 2009. Analytical derivation of the Budyko curve based on rainfall characteristics and a simple evaporation model. Water Resour Res 45. https://doi.org/10.1029/2008WR007308

Good, S.P., Moore, G.W., Miralles, D.G., 2017. A mesic maximum in biological water use demarcates biome sensitivity to aridity shifts. Nat Ecol Evol 1, 1883–1888. https://doi.org/10.1038/s41559-017-0371-8

465   Granier, A., 1985. Une nouvelle méthode pour la mesure du flux de sève brute dans le tronc des arbres. Annales des Sciences Forestières 42, 193–200. https://doi.org/10.1051/forest:19850204

Green, S., Clothier, B., Jardine, B., 2003. Theory and Practical Application of Heat Pulse to Measure Sap Flow. Agron J 95, 1371–1379. https://doi.org/10.2134/agronj2003.1371

Griffis, T.J., 2013. Tracing the flow of carbon dioxide and water vapor between the biosphere and atmosphere: A review of

470   optical isotope techniques and their application. Agric For Meteorol 174–175, 85–109. https://doi.org/10.1016/J.AGRFORMET.2013.02.009

Gupta, H. V., Kling, H., Yilmaz, K.K., Martinez, G.F., 2009. Decomposition of the mean squared error and NSE performance criteria: Implications for improving hydrological modelling. J Hydrol (Amst) 377, 80–91. https://doi.org/10.1016/j.jhydrol.2009.08.003

475   Hassan, A., Prentice, I.C., Liang, X., 2024. Understanding the Variability in Potential Evapotranspiration (PET) Products for U.S. Watersheds, in: AGU24, 9-13 Dec 2024.

Huang, C.-W., Chu, C.-R., Hsieh, C.-I., Palmroth, S., Katul, G.G., 2015. Wind-induced leaf transpiration. Adv Water Resour 86, 240–255. https://doi.org/10.1016/j.advwatres.2015.10.009

Hurkmans, R.T.W.L., De Moel, H., Aerts, J.C.J.H., Troch, P.A., 2008. Water balance versus land surface model in the
480   simulation of Rhine river discharges. Water Resour Res 44. https://doi.org/10.1029/2007WR006168

Jackson, R.B., Canadell, J., Ehleringer, J.R., Mooney, H.A., Sala, O.E., Schulze, E.D., 1996. A global analysis of root distributions for terrestrial biomes. Oecologia 108, 389–411. https://doi.org/https://doi.org/10.1007/BF00333714

Kool, D., Agam, N., Lazarovitch, N., Heitman, J.L., Sauer, T.J., Ben-Gal, A., 2014. A review of approaches for evapotranspiration partitioning. Agric For Meteorol. https://doi.org/10.1016/j.agrformet.2013.09.003

485   Li, B., Ryu, Y., Jiang, C., Dechant, B., Liu, J., Yan, Y., Li, X., 2023. BESSv2.0: A satellite-based and coupled-process model for quantifying long-term global land–atmosphere fluxes. Remote Sens Environ 295. https://doi.org/10.1016/j.rse.2023.113696

Li, M., Wu, P., Ma, Z., Pan, Z., Lv, M., Yang, Q., Duan, Y., 2022. The Increasing Role of Vegetation Transpiration in Soil Moisture Loss across China under Global Warming. J Hydrometeorol 23, 253–274. https://doi.org/10.1175/JHM-D-21-0132.1

490   Li, X., Gentine, P., Lin, C., Zhou, S., Sun, Z., Zheng, Y., Liu, J., Zheng, C., 2019. A simple and objective method to partition evapotranspiration into transpiration and evaporation at eddy-covariance sites. Agric For Meteorol 265, 171–182. https://doi.org/10.1016/J.AGRFORMET.2018.11.017

Lim, K.J., Engel, B.A., Tang, Z., Choi, J., Kim, K.S., Muthukrishnan, S., Tripathy, D., 2005. AUTOMATED WEB GIS BASED HYDROGRAPH ANALYSIS TOOL, WHAT1. JAWRA Journal of the American Water Resources Association 41,
495   1407–1416. https://doi.org/10.1111/J.1752-1688.2005.TB03808.X

Lim, K.J., Park, Y.S., Kim, J., Shin, Y.C., Kim, N.W., Kim, S.J., Jeon, J.H., Engel, B.A., 2010. Development of genetic algorithm-based optimization module in WHAT system for hydrograph analysis and model application. Comput Geosci 36, 936–944. https://doi.org/10.1016/J.CAGEO.2010.01.004

Lin, C., Gentine, P., Huang, Y., Guan, K., Kimm, H., Zhou, S., 2018. Diel ecosystem conductance response to vapor pressure
500   deficit is suboptimal and independent of soil moisture. Agric For Meteorol 250–251, 24–34. https://doi.org/10.1016/J.AGRFORMET.2017.12.078

Liu, Y., Zhang, Y., Shan, N., Zhang, Z., Wei, Z., 2022. Global assessment of partitioning transpiration from evapotranspiration based on satellite solar-induced chlorophyll fluorescence data. J Hydrol (Amst) 612, 128044. https://doi.org/10.1016/J.JHYDROL.2022.128044

505   Lozanova, L., Zhiyanski, M., Vanguelova, E., Doncheva, S., Marinov, M.P., Lazarova, S., 2019. Dynamics and Vertical Distribution of Roots in European Beech Forests and Douglas Fir Plantations in Bulgaria. Forests 2019, Vol. 10, Page 1123 10, 1123. https://doi.org/10.3390/F10121123

Lu, X., Liu, Z., An, S., Miralles, D.G., Maes, W., Liu, Y., Tang, J., 2018. Potential of solar-induced chlorophyll fluorescence to estimate transpiration in a temperate forest. Agric For Meteorol 252, 75–87.

510   https://doi.org/10.1016/J.AGRFORMET.2018.01.017

Magliano, P.N., Giménez, R., Houspanossian, J., Páez, R.A., Nosetto, M.D., Fernández, R.J., Jobbágy, E.G., 2017. Litter is more effective than forest canopy reducing soil evaporation in Dry Chaco rangelands. Ecohydrology 10. https://doi.org/10.1002/eco.1879

Mao, J., Yan, B., 2019. Global Monthly Mean Leaf Area Index Climatology, 1981-2015.

515   https://doi.org/https://doi.org/10.3334/ORNLDAAC/1653

Martens, B., Miralles, D.G., Lievens, H., Van Der Schalie, R., De Jeu, R.A.M., Fernández-Prieto, D., Beck, H.E., Dorigo, W.A., Verhoest, N.E.C., 2017. GLEAM v3: Satellite-based land evaporation and root-zone soil moisture. Geosci Model Dev 10, 1903–1925. https://doi.org/10.5194/GMD-10-1903-2017

Medlyn, B.E., Duursma, R.A., Eamus, D., Ellsworth, D.S., Prentice, I.C., Barton, C.V.M., Crous, K.Y., de Angelis, P.,

520   Freeman, M., Wingate, L., 2011. Reconciling the optimal and empirical approaches to modelling stomatal conductance. Glob Chang Biol 17, 2134–2144. https://doi.org/10.1111/J.1365-2486.2010.02375.X

Mesinger, F., DiMego, G., Kalnay, E., Mitchell, K., Shafran, P.C., Ebisuzaki, W., Jović, D., Woollen, J., Rogers, E., Berbery, E.H., Ek, M.B., Fan, Y., Grumbine, R., Higgins, W., Li, H., Lin, Y., Manikin, G., Parrish, D., Shi, W., 2006. North American Regional Reanalysis. Bull Am Meteorol Soc 87, 343–360. https://doi.org/10.1175/BAMS-87-3-343

525   Mianabadi, A., Coenders-Gerrits, M., Shirazi, P., Ghahraman, B., Alizadeh, A., 2019. A global Budyko model to partition evaporation into interception and transpiration. Hydrol. Earth Syst. Sci 23, 4983–5000. https://doi.org/10.5194/hess-23-4983-2019

Moran, M.S., Scott, R.L., Keefer, T.O., Emmerich, W.E., Hernandez, M., Nearing, G.S., Paige, G.B., Cosh, M.H., O'Neill, P.E., 2009. Partitioning evapotranspiration in semiarid grassland and shrubland ecosystems using time series of soil surface

530   temperature. Agric For Meteorol 149, 59–72. https://doi.org/10.1016/J.AGRFORMET.2008.07.004

Niu, Z., He, H., Zhu, G., Ren, X., Zhang, L., Zhang, K., Yu, G., Ge, R., Li, P., Zeng, N., Zhu, X., 2019. An increasing trend in the ratio of transpiration to total terrestrial evapotranspiration in China from 1982 to 2015 caused by greening and warming. Agric For Meteorol 279, 107701. https://doi.org/10.1016/J.AGRFORMET.2019.107701

Pagán, B.R., Maes, W.H., Gentine, P., Martens, B., Miralles, D.G., 2019. Exploring the Potential of Satellite Solar-Induced

535   Fluorescence to Constrain Global Transpiration Estimates. Remote Sensing 2019, Vol. 11, Page 413 11, 413. https://doi.org/10.3390/RS11040413

Ponce, V.M., Shetty, A. V., 1995a. A conceptual model of catchment water balance: 1. Formulation and calibration. J Hydrol (Amst) 173, 27–40. https://doi.org/10.1016/0022-1694(95)02739-C

Ponce, V.M., Shetty, A. V., 1995b. A conceptual model of catchment water balance: 2. Application to runoff and baseflow

540   modeling. J Hydrol (Amst) 173, 41–50. https://doi.org/10.1016/0022-1694(95)02745-B

Pool, S., Vis, M., Seibert, J., 2018. Evaluating model performance: towards a non-parametric variant of the Kling-Gupta efficiency. Hydrological Sciences Journal 63, 1941–1953. https://doi.org/10.1080/02626667.2018.1552002

Poyatos, R., Granda, V., Flo, V., Adams, M.A., Adorján, B., Aguadé, D., Aidar, M.P.M., Allen, S., Alvarado-Barrientos, M.S., Anderson-Teixeira, K.J., Aparecido, L.M., Altaf Arain, M., Aranda, I., Asbjornsen, H., Baxter, R., Beamesderfer, E., Berry, Z.C., Berveiller, D., Blakely, B., Boggs, J., Bohrer, G., Bolstad, P. v., Bonal, D., Bracho, R., Brito, P., Brodeur, J., Casanoves, F., Chave, J., Chen, H., Cisneros, C., Clark, K., Cremonese, E., Dang, H., David, J.S., David, T.S., Delpierre, N., Desai, A.R., Do, F.C., Dohnal, M., Domec, J.C., Dzikiti, S., Edgar, C., Eichstaedt, R., El-Madany, T.S., Elbers, J., Eller, C.B., Euskirchen, E.S., Ewers, B., Fonti, P., Forner, A., Forrester, D.I., Freitas, H.C., Galvagno, M., Garcia-Tejera, O., Ghimire, C.P., Gimeno, T.E., Grace, J., Granier, A., Griebel, A., Guangyu, Y., Gush, M.B., Hanson, P.J., Hasselquist, N.J., Heinrich, I., Hernandez-Santana, V., Herrmann, V., Hölttä, T., Holwerda, F., Irvine, J., Na Ayutthaya, S.I., Jarvis, P.G., Jochheim, H., Joly, C.A., Kaplick, J., Kim, H.S., Klemedtsson, L., Kropp, H., Lagergren, F., Lane, P., Lang, P., Lapenas, A., Lechuga, V., Lee, M., Leuschner, C., Limousin, J.M., Linares, J.C., Linderson, M.L., Lindroth, A., Llorens, P., López-Bernal, Á., Loranty, M.M., Lüttschwager, D., MacInnis-Ng, C., Maréchaux, I., Martin, T.A., Matheny, A., McDowell, N., McMahon, S., Meir, P., Mészáros, I., Migliavacca, M., Mitchell, P., Mölder, M., Montagnani, L., Moore, G.W., Nakada, R., Niu, F., Nolan, R.H., Norby, R., Novick, K., Oberhuber, W., Obojes, N., Oishi, A.C., Oliveira, R.S., Oren, R., Ourcival, J.M., Paljakka, T., Perez-Priego, O., Peri, P.L., Peters, R.L., Pfautsch, S., Pockman, W.T., Preisler, Y., Rascher, K., Robinson, G., Rocha, H., Rocheteau, A., Röll, A., Rosado, B.H.P., Rowland, L., Rubtsov, A. v., Sabaté, S., Salmon, Y., Salomón, R.L., Sánchez-Costa, E., Schäfer, K.V.R., Schuldt, B., Shashkin, A., Stahl, C., Stojanović, M., Suárez, J.C., Sun, G., Szatniewska, J., Tatarinov, F., TesaÅ™, M., Thomas, F.M., Tor-Ngern, P., Urban, J., Valladares, F., van der Tol, C., van Meerveld, I., Varlagin, A., Voigt, H., Warren, J., Werner, C., Werner, W., Wieser, G., Wingate, L., Wullschleger, S., Yi, K., Zweifel, R., Steppe, K., Mencuccini, M., Martínez-Vilalta, J., 2021. Global transpiration data from sap flow measurements: The SAPFLUXNET database. Earth Syst Sci Data 13, 2607–2649. https://doi.org/10.5194/ESSD-13-2607-2021

Running, S., Mu, Q., Zhao, M., Moreno, A., 2021. MODIS/Terra Net Evapotranspiration Gap-Filled Yearly L4 Global 500m SIN Grid V061 [Data set] [WWW Document]. URL https://doi.org/10.5067/MODIS/MOD16A3GF.061 (accessed 10.5.22).

Sakuratani, T., 1987. Studies on Evapotranspiration from Crops (2) Separate Estimation of Transpiration and Evaporation from a Soybean Field without Water Shortage. Journal of Agricultural Meteorology 42, 309–317. https://doi.org/10.2480/AGRMET.42.309

Sakuratani, T., 1981. A Heat Balance Method for Measuring Water Flux in the Stem of Intact Plants. Journal of Agricultural Meteorology 37, 9–17. https://doi.org/10.2480/AGRMET.37.9

Savenije, H.H.G., 2004. The importance of interception and why we should delete the term evapotranspiration from our vocabulary. Hydrol Process 18, 1507–1511. https://doi.org/10.1002/hyp.5563

Scanlon, T.M., Kustas, W.P., 2012. Partitioning Evapotranspiration Using an Eddy Covariance-Based Technique: Improved Assessment of Soil Moisture and Land–Atmosphere Exchange Dynamics. Vadose Zone Journal 11. https://doi.org/10.2136/VZJ2012.0025/111632

575   Scanlon, T.M., Kustas, W.P., 2010. Partitioning carbon dioxide and water vapor fluxes using correlation analysis. Agric For Meteorol 150, 89–99. https://doi.org/10.1016/J.AGRFORMET.2009.09.005

Scanlon, T.M., Sahu, P., 2008. On the correlation structure of water vapor and carbon dioxide in the atmospheric surface layer: A basis for flux partitioning. Water Resour Res 44, 10418. https://doi.org/10.1029/2008WR006932

Schenk, H.J., Jackson, R.B., 2002. The Global Biogeography of Roots. Ecol Monogr 72, 311–328.
580   https://doi.org/https://doi.org/10.1890/0012-9615(2002)072[0311:TGBOR]2.0.CO;2

Schlesinger, W.H., Jasechko, S., 2014. Transpiration in the global water cycle. Agric For Meteorol 189–190, 115–117. https://doi.org/10.1016/j.agrformet.2014.01.011

Schymanski, S.J., Or, D., 2016. Wind increases leaf water use efficiency. Plant Cell Environ 39, 1448–1459. https://doi.org/10.1111/pce.12700

585   Scott, R.L., Biederman, J.A., 2017. Partitioning evapotranspiration using long-term carbon dioxide and water vapor fluxes. Geophys Res Lett 44, 6833–6840. https://doi.org/10.1002/2017GL074324

Shan, N., Ju, W., Migliavacca, M., Martini, D., Guanter, L., Chen, J., Goulas, Y., Zhang, Y., 2019. Modeling canopy conductance and transpiration from solar-induced chlorophyll fluorescence. Agric For Meteorol 268, 189–201. https://doi.org/10.1016/J.AGRFORMET.2019.01.031

590   Skaggs, T.H., Anderson, R.G., Alfieri, J.G., Scanlon, T.M., Kustas, W.P., 2018. Fluxpart: Open source software for partitioning carbon dioxide and water vapor fluxes. Agric For Meteorol 253–254, 218–224. https://doi.org/10.1016/J.AGRFORMET.2018.02.019

Stocker, B.D., Wang, H., Smith, N.G., Harrison, S.P., Keenan, T.F., Sandoval, D., Davis, T., Prentice, I.C., 2020. P-model v1.0: An optimality-based light use efficiency model for simulating ecosystem gross primary production. Geosci Model Dev
595   13, 1545–1581. https://doi.org/10.5194/gmd-13-1545-2020

Stoy, P.C., El-Madany, T.S., Fisher, J.B., Gentine, P., Gerken, T., Good, S.P., Klosterhalfen, A., Liu, S., Miralles, D.G., Perez-Priego, O., Rigden, A.J., Skaggs, T.H., Wohlfahrt, G., Anderson, R.G., Coenders-Gerrits, A.M.J., Jung, M., Maes, W.H., Mammarella, I., Mauder, M., Migliavacca, M., Nelson, J.A., Poyatos, R., Reichstein, M., Scott, R.L., Wolf, S., 2019. Reviews and syntheses: Turning the challenges of partitioning ecosystem evaporation and transpiration into opportunities.
600   Biogeosciences 16, 3747–3775. https://doi.org/10.5194/BG-16-3747-2019

Swanson, R.H., Whitfield, D.W.A., 1981. A Numerical Analysis of Heat Pulse Velocity Theory and Practice. J Exp Bot 32, 221–239. https://doi.org/10.1093/JXB/32.1.221

Tan, S., Wang, H., Prentice, I.C., Yang, K., 2021. Land-surface evapotranspiration derived from a first-principles primary production model. Environmental Research Letters 16, 104047. https://doi.org/10.1088/1748-9326/ac29eb

605   Tang, Y., and D. Wang (2017), Evaluating the role of watershed properties in long-term water balance through a Budyko equation based on two-stage partitioning of precipitation, Water Resour. Res., 53, doi:10.1002/2016WR019920.

Thornton, M.M., Shrestha, R., Wei, Y., Thornton, P.E., Kao, S.-C., Wilson, B.E., 2022. Daymet: Daily Surface Weather Data on a 1-km Grid for North America, Version 4 R1. https://doi.org/10.3334/ORNLDAAC/2129

Wallace, A., Romney, E.M., Cha, J.W., 1980. DEPTH DISTRIBUTION OF ROOTS OF SOME PERENNIAL PLANTS IN
610   THE NEVADA TEST SITE AREA OF THE NORTHERN MOJAVE DESERT. Great Basin Naturalist Memoirs 201–207.

Wang, D., and Y. Tang (2014), A oneparameter Budyko model for water balance captures emergent behavior in darwinian
hydrologic models, Geophys. Res. Lett., 41, doi:10.1002/2014GL060509.

Wang, H., Prentice, I.C., Keenan, T.F., Davis, T.W., Wright, I.J., Cornwell, W.K., Evans, B.J., Peng, C., 2017. Towards a
universal model for carbon dioxide uptake by plants. Nat Plants 3, 734–741. https://doi.org/10.1038/s41477-017-0006-8

615   Wang, L., Good, S.P., Caylor, K.K., 2014. Global synthesis of vegetation control on evapotranspiration partitioning. Geophys
Res Lett 41, 6753–6757. https://doi.org/10.1002/2014GL061439

Wei, Z., Yoshimura, K., Wang, L., Miralles, D.G., Jasechko, S., Lee, X., 2017. Revisiting the contribution of transpiration to
global terrestrial evapotranspiration. Geophys Res Lett 44, 2792–2801. https://doi.org/10.1002/2016GL072235

Williams, D.G., Cable, W., Hultine, K., Hoedjes, J.C.B., Yepez, E.A., Simonneaux, V., Er-Raki, S., Boulet, G., de Bruin,
620   H.A.R., Chehbouni, A., Hartogensis, O.K., Timouk, F., 2004. Evapotranspiration components determined by stable isotope,
sap   flow   and   eddy   covariance   techniques.   Agric   For   Meteorol   125,   241–258.
https://doi.org/10.1016/J.AGRFORMET.2004.04.008

Yu, L., Zhou, S., Zhao, X., Gao, X., Jiang, K., Zhang, B., Cheng, L., Song, X., Siddique, K.H.M., 2022. Evapotranspiration
Partitioning   Based   on   Leaf   and   Ecosystem   Water   Use   Efficiency.   Water   Resour   Res   58.
625   https://doi.org/10.1029/2021WR030629

Zeng, X., 2001. Global Vegetation Root Distribution for Land Modeling. J Hydrometeorol 2, 525–530.
https://doi.org/https://doi.org/10.1175/1525-7541(2001)002%3C0525:GVRDFL%3E2.0.CO;2

Zhang, K., Kimball, J.S., Nemani, R.R., Running, S.W., 2010. A continuous satellite-derived global record of land surface
evapotranspiration from 1983 to 2006. Water Resour Res 46, 9522. https://doi.org/10.1029/2009WR008800

630   Zhang, Y., Shen, Y., Sun, H., Gates, J.B., 2011. Evapotranspiration and its partitioning in an irrigated winter wheat field: A
combined   isotopic   and   micrometeorologic   approach.   J   Hydrol   (Amst)   408,   203–211.
https://doi.org/10.1016/J.JHYDROL.2011.07.036

Zhou, S., Yu, B., Zhang, Y., Huang, Y., Wang, G., 2016. Partitioning evapotranspiration based on the concept of underlying
water use efficiency. Water Resour Res 52, 1160–1175. https://doi.org/10.1002/2015WR017766

635